Journal of
NANOSTRUCTURES
JNS
NANOSTRUCTURES
JNS.kashanu.ac.ir

Nanosheets of BiOCl Incorporated in Microflowers: Microwave Assisted Synthesis and Dye-Photosensitized Removal of Pollutants

A. Tadjarodi[a,*] , O. Akhavan[b,c], K. Bijanzad[a]

[a]*Research Laboratory of Inorganic Materials Synthesis, Department of Chemistry, Iran University of Science and Technology, Narmak, Tehran 16846-13114, Iran*

[b]*Department of Physics, Sharif University of Technology, P.O. Box 11155-9161, Tehran, Iran*

[c]*Institute for Nanoscience and Nanotechnology, Sharif University of Technology, P.O. Box 14588-89694, Tehran, Iran*

Article history:
Received 10/12/2014
Accepted 18/01/2015
Published online 1/03/2015

Keywords:
Bismuth oxychloride
Microflower
Microwave
Nanosheets
Semiconductor

**Corresponding author*
E-mail address:
tajarodi@iust.ac.ir
Tel.: +98 21 77240516
fax: +98 21 77491204

Abstract

BiOCl microflowers were synthesized using bismuth nitrate pentahydrate and sodium chloride by microwave (MW) assisted synthesis method for 23 minutes at 180 W. Scanning electron microscopy (SEM) studies revealed a unique morphology of flower-like assemblies comprised of nanosheets. The X-ray diffraction (XRD) pattern showed that a highly pure and crystalline phase has been obtained. The energy dispersive X-ray (EDS) and photoluminescence (PL) and Fourier transform infrared (FTIR) spectroscopies were also used to evaluate the composition and structure of the product. The UV-vis diffuse reflectance spectroscopy (DRS) studies revealed the indirect band gap value of about 3.33 eV for the fabricated semiconductor. Photocatalytic studies confirmed that the BiOCl nanostructure could remove Rhodamine B (RhB) and Natural Red 4 (N-Red) dyes from the aqueous solutions by dye-photosensitized degradation mechanism under visible light illumination.

1. Introduction

Semiconductors have been applied in different fields such as protein degradation, photoinactivation of bacteria, photo stimulation of human neural stem cells and photodegradation of textile dyes [1-5]. Scientists have recently paid a particular attention to the nanostructured photocatalysts since the chemical activity

increases in the nanoscale [6]. To date, various bismuth-based semiconductors such as $BiErWO_6$ [7], Bi [8], Au–Bi_2S_3 [9] and $BiNbO_4$ [10] have revealed an efficient photocatalytic activity in the removal of toxic textile dyes and other pollutants. Kudo *et al.* found the efficient photocatalytic activity of Bi-based semiconductors for the first time [11] and BiOCl was the first bismuth oxyhalide (BiOX) used as the photocatalyst [12]. It is clarified that the exceptional properties of BiOCl come from the weak interlayer van der Waals interaction and the strong intralayer bonding between $[Bi_2O_2]$ sheets and Cl slabs [13]. Until now, various scenarios have been applied to fabricate different compositions of BiOCl nanostructures with the enhanced activities. It is reported that three dimensional hierarchical architectures of BiOCl have been prepared using dioctyl sulfosuccinate and its gas sensing properties was studied [14]. Sarwan et. al. [15] prepared gray BiOCl by hydrolysis and UV light irradiation methods and investigated the effect of oxygen vacancies on its improved visible light photocatalytic activity as compared to the white BiOCl. Black BiOCl was synthesized by Li et. al. [16] by iron reduction and it showed a suitable visible light photocatalytic performance as a consequence of disordered surface structure. Also, it is clarified that the ultrathin nanosheets in the structure of $TiO_2/Bi_2(BDC)_3/BiOCl$ (BDC=1,4-benzenedicarboxylate) are responsible for the excellent photocatalytic activity [17]. In addition, structures such as Bi_2S_3-sensitized BiOCl [18], Fe,Nb-doped BiOCl [19], Cu-modified BiOCl [20] and C_3N_4-BiOCl [21] have been lately prepared and evaluated. It is also reported that compositions like Bi_3O_4Cl could degrade methyl orange more efficiently than TiO_2 under UV light illumination. The effective electron-hole pairs separation occur as a result of the internal electric fields between $[Bi_3O_4]$ and [Cl] slabs and also the hybrid states at the conduction and valence bands [22]. The use of nitric acid and different templates and the necessity of the precise control of solution acidity for the facbrication of BiOCl nanostructures have motivated the scientists to explore new preparation methods such as microwave synthesis. The heating effect of microwaves for the first time was accidentally discovered by Percy Le Baron Spencer in 1945 [23]. Hayes [24] described the microwave synthesis as "chemistry at the speed of light". The microwave preparation technology has been started in inorganic chemistry since the late 1970s [25] and the main advantages of it include: 1) Microwave energy increases the heating rate of the synthesis media and therefore, the reaction rate will increase. 2) It provides a more uniform heating. 3) It can superheat the reagents. 4) Hot spots are produced within the synthesis mixture. 5) It enhances the dissolution of reagents [26].

In this research, microwave assisted synthesis of BiOCl by using only bismuth nitrate, sodium chloride and water is reported. The photocatalytic performance of the product for degradation of RhB and N-Red dyes have been evaluated. The product was characterized by FTIR, XRD, SEM, EDS, DRS and PL.

2. Experimental section

2.1. Chemicals and synthesis

Bismuth nitrate pentahydrate (98.0%) was purchased from SAMCHUN CHEMICALS, Korea.

All the other reagents were purchased from Merck Company and used without further purification. RhB and N-Red [27] dyes were used as the model pollutants and deionized (DI) water was used to prepare the dye solutions. $Bi(NO_3)_3{\cdot}5H_2O$ (2.91 g) and NaCl (0.116 g) in DI water (20 mL) were used as the initial reagents to fabricate the product. The reaction was carried out in a domestic microwave instrument (Household microwave oven, Samsung GE 280, Frequency 2.45 GHz and a maximum output of 900 W) at 180 W for 23 minutes in a pyrex container (open atmosphere) then cooled to room temperature naturally. It is noteworthy that microwave heating at high temperatures may become somewhat difficult for pure water and therefore, temperature control of the reaction is necessary by periodic delays during the synthesis [23]. Therefore, we had a 3 min delay after every 2 min microwave processing. It is proved that the higher and uniform heating rates is observed at the edges rather than the center and hence, the load is placed on the edge of the turntable [28]. Before starting the procedure, the mixture was stirred for 10 min to have a homogenous solution. The final product was washed with DI water for several times to purify the products from the initial reagents or possible by-products and dried at room temperature.

2.2. Characterization

FTIR spectrum was recorded in the range of 400–4000 cm^{-1} on a Shimadzu-8400S spectrometer using KBr pellets. The powder XRD measurement was performed using a JEOL diffractometer with monochromatic Cu Kα radiation (λ=1.5418 Å). SEM images of the produced BiOCl were taken by VEGA/TESCAN microscope with an accelerating voltage of 30.00 kV. The energy dispersive X-ray spectroscopy was taken on a Philips (XL-30) with gold coating to discover the elements present in the product. DRS spectrum was prepared by a Shimadzu (MPC-2200) spectrophotometer. The room temperature photoluminescence spectrum was taken on a PL-Perkin-Elmer LS55 equipped with a 450 W Xe lamp as excitation source (excitation wavelength= 200 nm). The UV-vis absorption studies were carried out at room temperature in the wavelength range of the 190–800 nm on a UV-vis spectrometer (Shimadzu UV–1700).

2.3. Photocatalytic test

RhB and N-Red were used as the representative pollutants to analyze the photocatalytic performance of the as-prepared BiOCl. The photodegradation experiments were carried out under the following conditions: 0.05 g of the photocatalyst was added to 100 mL of dye aqueous solutions with the initial concentrations of 10 mg L^{-1} at room temperature and neutral pH. The suspensions were stirred using a magnetic stirrer for 1 h in the dark to adjust an adsorption-desorption equilibrium. The concentration values of the residual dyes were measured using UV–vis spectrophotometer at the appropriate wavelengths corresponding to the maximum absorptions of RhB (554 nm) and N-Red (525 nm). The reaction vessel was then placed under light irradiation in the photo-reactor to continue the photodegradation process. The visible light irradiation was supplied using a source of 500 W high-pressure mercury-vapor lamp (λ= 546.8 nm), mounted 10 cm from the reaction solution. The mercury lamp (HWL 500 W, 225 V, E40) was purchased from the

OSRAM Co. of China. The RhB and N-Red solutions were kept at room temperature during the photocatalytic process by a water bath equipped with a circulating system. At specific time intervals of irradiation, the portions of suspension were taken from the reaction vessel, centrifuged at 14000 rpm for 10 min and analyzed by UV-vis spectrophotometer.

3. Results and discussion

3.1. Compositional characterization, morphological and optical studies

The microwave irradiation has great advantages over conventional heating including the selective activation of the precursors to initiate the nucleation and growth and morphological control [29]. It also provides more uniform seeds and also highly crystalline and faceted nanoparticles [30]. Microwave synthesis in a domestic microwave oven is an easy, cost effective and programmable preparation method [31-34]. It is reported a rate enhancement of 5 to 1240 times in case of several organic reactions. The "specific microwave effects" and the "nonthermal microwave effects" are involved in the synthesis process but it is very complicated to measure the exact magnitude of each effect. The MW heating operates by two main mechanisms, dipolar polarization and ionic conduction. Water is a polar solvent and a good microwave absorber and most studies have been devoted to the microwave synthesis of inorganic materials in the aqueous solution. Furthermore, the presence of ions in the solution could play a significant role in the approach of maximum heating rate [23].

The functional groups and chemical bonds of the product were evaluated by Fourier transform infrared spectroscopy. FTIR spectrum of the product is shown in Fig. 1. The peak at 570 cm^{-1} was attributed to the stretching vibrations of the Bi—O bond. The bands at 1627 cm^{-1} and 1355 cm^{-1} are ascribed to the adsorbed atmospheric CO_2 resulted from the synthesis procedure and processing of FTIR sample. The peak at 1460 cm^{-1} is assigned to the bending vibrations of O—H groups of adsorbed water molecules and the corresponding stretching vibrations are appeared at 3531 cm^{-1}. The surface hydroxyl groups from the adsorbed water molecules could enhance the photocatalytic activity [35-37].

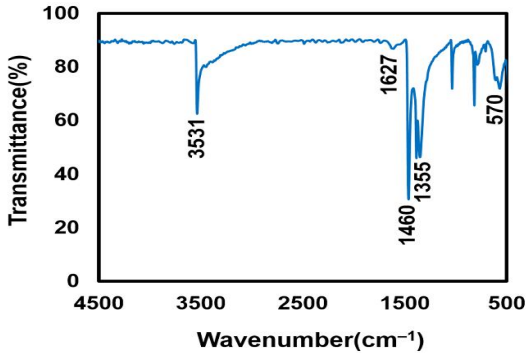

Fig. 1. FTIR spectrum of BiOCl nanostructure.

The XRD analysis was used to study the composition of the product (Fig. 2). The reflections of the product could be indexed to the tetragonal phase of BiOCl pattern (JCPDS card No. 006-0249) with the space group of P4/nmm and lattice parameters of a=3.89 Å, b=3.89 Å, c=7.37 Å and α=β=γ=90°. The diffraction peaks at 2θ values of 11.98°, 24.10°, 25.86°, 32.50°, 33.45°, 40.90°, 46.64°, 49.70°, 54.10°, 55.12° and 58.60° match the respective (001), (002), (101), (110), (102), (112), (200), (113), (211), (104) and (212) planes of tetragonal bismuth

oxychloride well. The sharp reflections of the product indicates its high purity and single phase.

Figures 3(a-c) show the SEM images of the BiOCl synthesized by microwave-assisted method. As it is clear, the product consists of a large number of irregular nanosheets. Although the morphology of BiOCl hierarchical structures is not uniform completely, a specific flower-like assembly of nanosheets is observed which are not highly close packed. The separated nanosheets provide more active sites for interaction with the pollutant molecules. In the high-magnification SEM image (Figs. 2(b,c)), a unique flower-like morphology with an average diameter of 2 μm can be clearly seen which is comprised of numerous BiOCl nanosheets with a thickness of *ca.* 30-50 nm. It is suggested that the two dimensional nanosheets were formed as a result of the van der Waals forces through Cl atoms in the atomic layers of [Cl–Bi–O–Bi–Cl] [20]. Subsequently, these sheets were packed on each other to construct a 3D flower-like morpholgy. It is known that the amount of halide in the composition of BiOX is a crucial factor that influences the morphology and size of the bismuth oxyhalides [38]. Also, the hydrogen bonds formed between different hydroxylated surfaces and water molecules could have a special effect on the morphlogy [39,40].

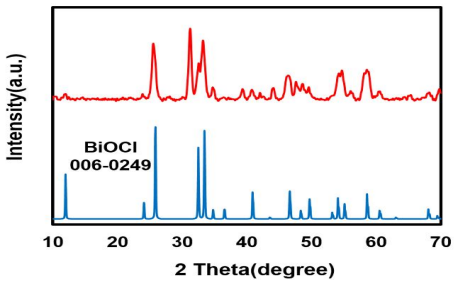

Fig. 2. XRD patterns of as-prepared BiOCl and BiOCl with JCPDS card No. 006-0249.

To confirm the presence of elements, we have done the EDS analysis for the product. The elemental analysis for the as-prepared BiOCl, as measured by EDS in SEM, is shown in Fig. 3d. It is seen that the sample was composed of three main elements–bismuth, oxygen and chlorine and the atomic ratios of Bi:O:Cl were 72.72:5.24:22.04. These results further confirmed the high purity of the produced BiOCl.

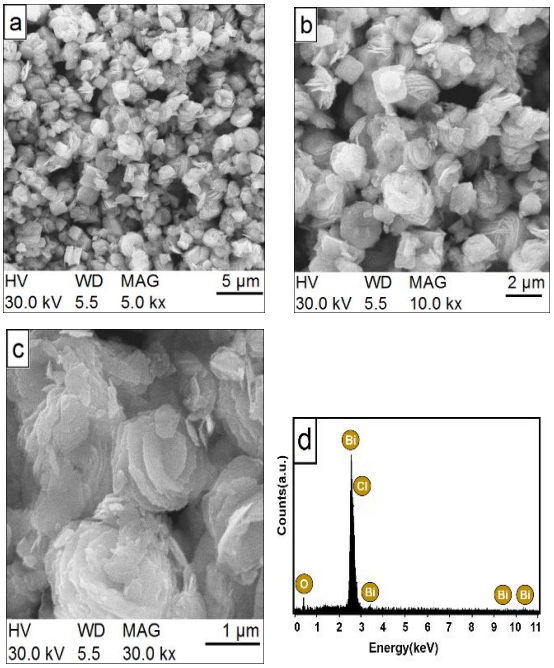

Fig. 3. SEM images (a-c) and EDS analysis (d) of BiOCl nanostructure.

The UV–vis diffuse reflectance spectrum of the synthesized flower-like BiOCl is shown in Fig. 4. Applying the optical absorption data near the band edge, the band-gap value was calculated according to the following empirical equation:

$$\alpha h\nu = A(h\nu - Eg)^{n/2} \quad \text{(Eq. 1)}$$

where α, v, A, and Eg are the absorption coefficient, light frequency, proportionality constant, and band gap, respectively.

In Eq. 1, n identifies whether the transition in a semiconductor is direct (n=1) or indirect (n=4). The values of n and Eg are determined through the following steps: (1) assuming an approximate Eg value, $ln(\alpha hv)$ versus $ln(hvEg)$ should be plotted and the value of n could be determined from the slope of the straightest line near the band edge, (2) $(\alpha hv)^{2/n}$ versus hv should be plotted and then calculate the band gap, Eg, by extrapolating the straightest line to the hv axis intercept [41]. The value of n for the product was 4 and therefore, it is an indirect band gap semiconductor and the value of the band gap was estimated to be 3.33 eV. It is known that morphology, surface area, surface defects and composition of the photocatalysts highly influence the band gap and hence the photocatalytic acitivity [41,42]. To study the effect of the above-mentioned factors, the photocatalytic activity of the as-prepared BiOCl toward RhB and N-Red photodegradation was investigated.

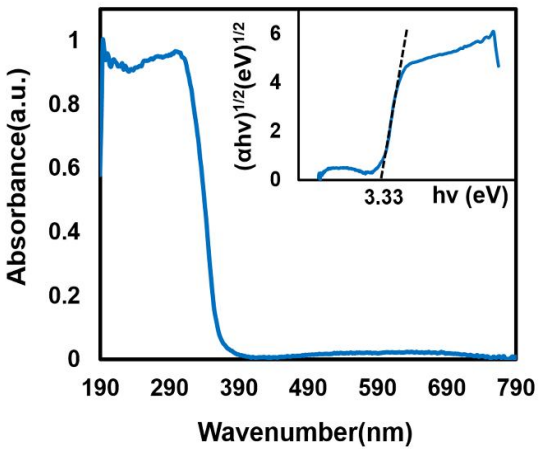

Fig. 4. UV-vis absorption spectrum of BiOCl nanostructure (inset shows plot of $(\alpha hv)^{1/2}$ *vs.* hv).

3.2. Photocatalytic activity

3.2.1. Photocatalytic experiment

Photocatalytic performance of the product was evaluated by photodegradation process of RhB and N-Red dyes from the aqueous solutions. The degradation efficiency is calculated by Eq. 2:

$$\%\ Degradation\ Efficiency = (C_0\text{-}C)/C_0 \times 100 \quad \text{(Eq. 2)}$$

Where, C_0 is the initial concentration of dye and C is the concentration of dye after treatment at different times, t (0-5 h). The experimental results showed that the maximum degradation efficiency of RhB and N-Red after 5 h illumination by BiOCl were 78.12 and 55.54 %, respectively (Fig. 5). The adsorption-desorption equilibrium section in the dark (1th hour of the process) showed the reduction of N-Red concentration was higher than the RhB dye which is related to the structure of the dyes (Fig. 6) [43].

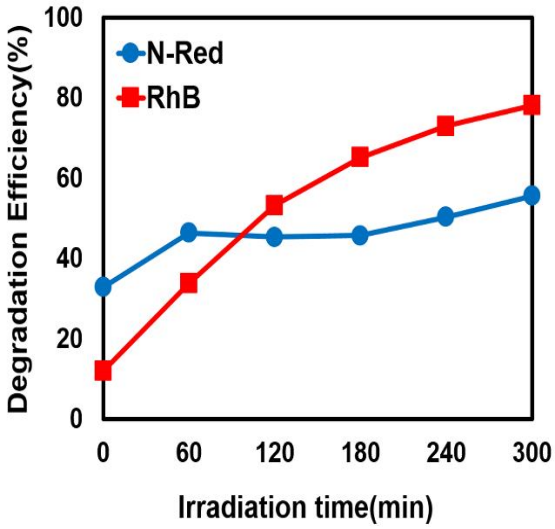

Fig. 5. Photocatalytic degradation curves of BiOCl nanostructure toward RhB and N-Red.

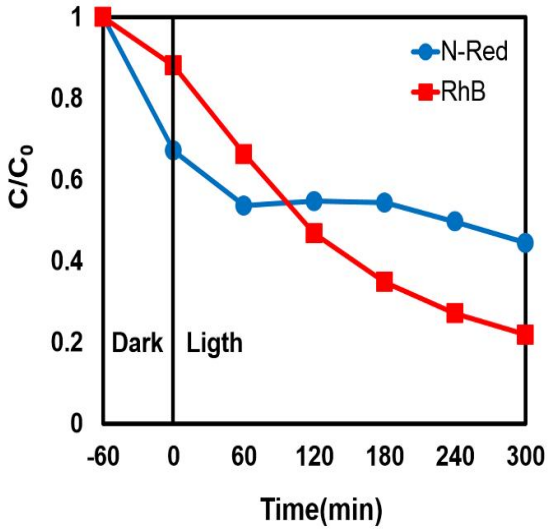

Fig. 6. Comparison of RhB and N-Red photodegradations by BiOCl nanostructure.

A superior degradation efficiency of dye molecules is observed under visible light irradiation which is mainly ascribed to the photocatalytic activity of bismuth oxychloride. The absorption spectra of RhB and N-Red over BiOCl in the photocatalytic reactions are given in Fig. 7. A fast decrease of absorptions for RhB (at λ=554 nm) and N-Red (at λ=525 nm) along with an absorption band shift to shorter wavelengths (hypsochromic shift) for RhB dye molecules were observed [41]. A possible mechanism for RhB photodegradation is based on de-ethylation and carboxylation of the dye molecules and the intermediates and it is finally mineralized to CO_2 and H_2O.

The gradual hypsochromic shift of the main absorption peak of RhB was ascribed to the step-by-step de-ethylation of dye molecules and the reduction in absorbance intensities is attributed to the destruction of the conjugated structure [42].

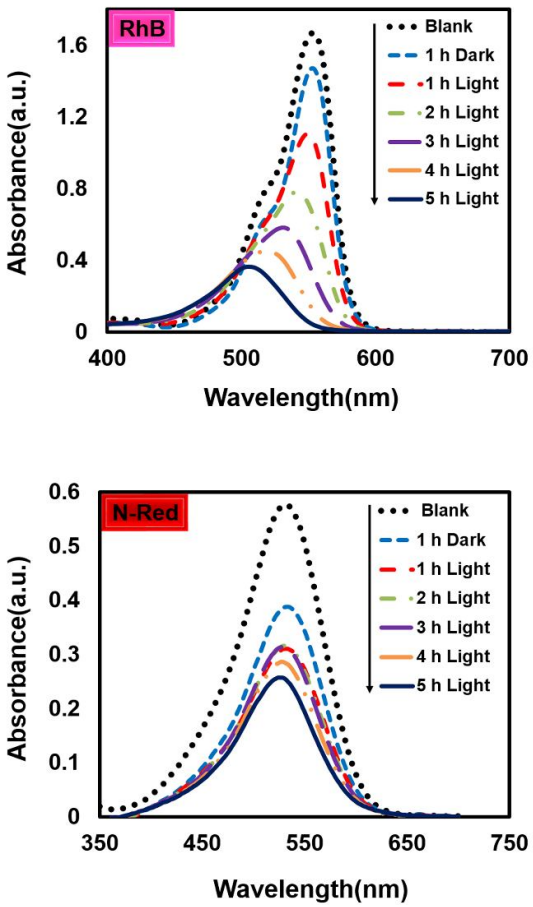

Fig. 7. UV absorption spectra of RhB (up) and N-Red (down) by BiOCl under visible light for 5 h.

3.2.2. Photocatalytic reaction kinetics

The photodegradation rates of RhB and N-Red dyes by BiOCl were recorded at different times to study the kinetics of photocatalytic processes. The results revealed a linear relationship between $ln(C_0/C)$ versus reaction time, t, (Fig. 8) which can be described by the pseudo-first-order kinetic model (Eq. 3).

$$ln(C_0/C)=kt \qquad \text{(Eq. 3)}$$

Where C_0 is the initial concentration (mM), C is the instantaneous concentration of the dye at different time intervals of illumination and the

slope, *k*, is the apparent rate constant. The rate constants of RhB and N-Red photodegradation reactions were 0.0047 and 0.0011 min^{-1}, respectively.

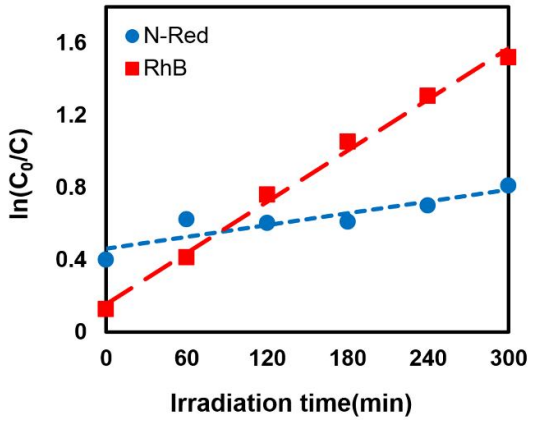

Fig. 8. Photocatalytic kinetics of photodegradation of RhB and N-Red dyes by BiOCl nanostructure.

Fig. 9 shows the photoluminescence spectrum of BiOCl nanostructure excited by 200 nm irradiation. It is clear that the main emission peak was centered at about 385 nm for the product. PL processes are very complicated and highly influenced by excitation energy, material size, composition and structure of the lattice [13,46].

Photoluminescence occurs as a result of band-band or excitonic processes. As clearly noticed in the diagram, the wavelength of PL signal for the produced bismuth oxychloride is higher than the wavelength of its band gap. Therefore, it is concluded that the excitonic PL process has been occurred. In an excitonic PL process, the non-radiative transitions of excited electrons from the conduction band bottom to different sub-bands or surface states occur first and then the radiative transitions from the sub-bands to the valence band top will take place, therefore, its energy would be lower than the band gap energy. Indeed, there are some sub-bands in the band gap resulted from the surface defects and surface states. The electrons of mid-gap states directly influence the electronic structure through formation of energy levels below the conduction band.

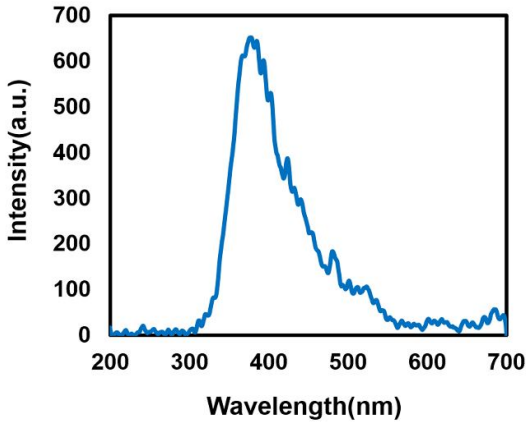

Fig. 9. Photoluminescence spectrum of BiOCl nanostructure.

It is known that the strong excitonic PL spectrum indicates the high content of surface oxygen vacancies and defects. The oxygen vacancies and defects will act as centers to seize the photo-induced electrons to inhibit the recombination of electrons and hole pairs, efficaciously. Oxygen vacancies can promote the O_2 adsorption and thus, the photo-induced electrons will interact strongly both with the oxygen vacancies and the adsorbed O_2 to generate superoxide radicals. From another point of view, a bulk semiconductor shows a weak PL signal or even no PL signal. Therefore, the strong PL intensity of the product is another sign of its nanostructure [16,40, 45-46].

3.2.3. Photodegradation mechanism

Bismuth-based photocatalysts show high activity because the Bi 6s and O 2p levels form

largely dispersed hybridized valence bands. The strong internal static electric fields between [Bi_2O_2] and [Cl] slabs are beneficial for the efficient separation of photo-induced electron–holes [22]. Additionally, long Bi—Cl bonds result in fair structure-openness degrees and wider spatial locations for atom vibrations. Consequently, the higher momentary polarizing fields will be generated in the irregular local structures and will support a fair mobility for the separation of electron–hole pairs in the semiconductor [47].

Direct photocatalytic or indirect photosensitized pathways or both of them may participate in photodegradation of dyes by BiOCl photocatalysts [38]. The dye-photosensitized degradation might be the only route for the produced bismuth oxychloride since the band gap does not correspond the visible light region. Therefore, the removal of RhB and N-Red dyes occurred via an indirect dye-photosensitized degradation pathway. In photosensitization mechanism, the dye self-sensitizes its own oxidative transformation by the indirect production of oxidizing $^{\bullet}OH$ radicals [42]. The hydroxyl radicals could be produced by multistep reduction of $O_2^{\bullet-}$. This is because as a result of more negative standard redox potential of Bi^{V}/Bi^{III} than $^{\bullet}OH/ OH^{-}$, bismuth oxyhalides are not capable of $^{\bullet}OH$ production [48]. Moreover, the surface hydroxyl groups and/or the chemisorbed water molecules on BiOCl will scavenge the holes and provide adsorption sites for reactants and intermediates [49]. Hydroxyl radicals might be also formed by the oxygen molecules dissolved in the solution [50]. In addition, the vacancies and defects can modify the adsorption capacity of gaseous molecules on the surface of photocatalysts and therefore, the superoxide anion radicals will be formed via O_2 capture. They might also extend the light-response edge of the photocatalyst to influence the band gap [6]. The positive charge of oxygen vacancies will only trap the electrons (and not the holes) and thus the recombination of electrons and hole pairs is reduced [51]. Also, the indirect band gap nature of bismuth oxyhalides, the unique 3D morphology [52,53] and the thin nanoplates will assist the photocatalytic activity [38].

Adsorption experiments were carried out by BiOCl nanostructure for 5 h in the dark. The results showed that adsorption process in 2^{nd} to 5^{th} hours was not more than the magnitude observed in the first hour. It confirms that the whole process occurred under the visible light was (dye-photosensitized) photocatalysis and not the adsorption.

4. Conclusions

Microflowers of BiOCl comprised of nanosheets were synthesized using a microwave assisted method. Photocatalytic studies showed that the BiOCl nanostructure with the band gap of 3.33 eV can remove RhB and N-Red dyes from the aqueous solutions by dye-photosensitized degradation mechanism under visible light illumination.

Acknowledgments

The authors would like to thank Iran University of Science and Technology, the Research Council of Sharif University of Technology and Iran Nanotechnology Initiative Council for financial support of the work.

References

[1] O. Akhavan, E. Ghaderi, Nanoscale 5 (2013) 10316-10326.
[2] O. Akhavan, R. Azimirad, S. Safa, Mater. Chem. Phys. 130 (2011) 598-602.
[3] O. Akhavan, M. Choobtashani, E. Ghaderi, J. Phys. Chem. C 116 (2012) 9653-9659.
[4] M. Zhang, Y. Liu, L. Li, H. Gao, X. Zhang, Catal. Comm. 58 (2015) 122-126.
[5] S. Weng, B. Chen, L. Xie, Z. Zheng, P. Liu, J. Mater. Chem. A 1 (2013) 3068-3075.
[6] J. Li, Y. Yu, L. Zhang, Nanoscale 6 (2014) 8473-8488.
[7] H. Du, J. Luan, Solid State Sci. 14 (2012) 1295-1305.
[8] Q. Zhang, Y. Zhou, F. Wang, F. Dong, W. Li, H. Li, G.R. Patzke, J. Mater. Chem. A 2 (2014) 11065-11072.
[9] G. Manna, R. Bose, N. Pradhan, Angew. Chem. Int. Ed. 53 (2014) 6743-6746.
[10] H.-F. Zhai, A.-D. Li, J.-Z. Kong, X.-F. Li, J. Zhao, B.-L. Guo, J. Yin, Z.-S. Li, D. Wu, J. Solid State Chem. 202 (2013) 6-14.
[11] A. Kudo, K. Omori, H. Kato, J. Am. Chem. Soc. 121 (1999) 11459-11467.
[12] H. An, Y. Du, T. Wang, C. Wang, W. Hao, J. Zhang, Rare Met. 27 (2008) 243-250.
[13] L. Armelao, G. Bottaro, C. Maccato, E. Tondello, Dalton Trans. 41 (2012) 5480-5485.
[14] C.R. Michel, N.L.L. Contreras, A.H. Martínez-Preciado, Sensor. Actuat. B-Chem. 160 (2011) 271-277.
[15] B. Sarwan, B. Pare, A.D. Acharya, Mater. Sci. Semicond. Process. 25 (2014) 89-97.
[16] Y. Li, C. Li, Z. Zhang, Y. Zhang, X. Sun, H. Si, J. Zhang, Solid State Sci. 34 (2014) 107-112.
[17] S.-M. Zhou, D.-K. Ma, P. Cai, W. Chen, S.-M. Huang, Mater. Res. Bull. 60 (2014) 64-71.
[18] J. Cao, B. Xu, H. Lin, B. Luo, S. Chen, Catal. Comm. 26 (2012) 204-208.
[19] M. Nussbaum, N. Shaham-Waldmann, Y. Paz, J. Photoch. Photobio. A 290 (2014) 11-21.
[20] J. Di, J. Xia, S. Yin, H. Xu, L. Xu, Y. Xu, M. He, H. Li, RSC Adv. 4 (2014) 14281-14290.
[21] L. Lei, H. Jin, Q. Zhang, J. Xu, D. Gao, Z. Fu, Dalton Trans. 44 (2015) 795-803.
[22] X. Lin, T. Huang, F. Huang, W. Wang, J. Shi, J. Phys. Chem. B 110 (2006) 24629-24634.
[23] Y.-J. Zhu, F. Chen, Chem. Rev. 114 (2014) 6462-6555.
[24] B. Hayes, Microwave Synthesis: Chemistry at the Speed of Light, CEM Publishing: Matthews, 2002.
[25] P. Lidström, J. Tierney, B. Wathey, J. Westman, Tetrahedron 57 (2001) 9225-9283.
[26] G.A. Tompsett, W.C. Conner, K.S. Yngvesson, Chem. Phys. Chem. 7 (2006) 296-319.
[27] M. Norman, P. Bartczak, J. Zdarta, W. Tylus, T. Szatkowski, A.L. Stelling, H. Ehrlich, T. Jesionowski, Materials 8 (2015) 96-116.
[28] E. Muthuswamy, A.S. Iskandar, M.M. Amador, S.M. Kauzlarich, Chem. Mater. 25 (2013) 1416-1422.
[29] S. Song, W. Gao, X. Wang, X. Li, D. Liu, Y. Xing, H. Zhang, Dalton Trans. 41 (2012) 10472-10476.
[30] N. Dahal, S. García, J. Zhou, S.M. Humphrey, ACS Nano 6 (2012) 9433-9446.
[31] H. Hu, X. Wang, F. Liu, J. Wang, C. Xu, Synthetic Met. 161 (2011) 404-410.
[32] A. Tadjarodi, A.H. Cheshmekhavar, M. Imani, Appl. Surf. Sci. 263 (2012) 449-456.
[33] T. Lin, Z. Liu, M. Zhou, H. Bi, K. Zhang, F. Huang, D. Wan, Y. Zhong, ACS App. Mater. Inter. 6 (2014) 3088-3092.
[34] Y. Choi, G.H. Ryu, S.H. Min, B.R. Lee, M.H. Song, Z. Lee, B.-S. Kim, ACS Nano 8 (2014) 11377-11385.
[35] K. Zhang, J. Huang, H. Wang, G. Yu, B. Wang, S. Deng, J. Kano, Q. Zhang, RSC Adv. 4 (2014) 14719-14724.

[36] M. Mączka, L. Kępiński, L. Macalik, J. Hanuza, Mater. Chem. Phys. 125 (2011) 93-101.
[37] F. Dong, T. Xiong, R. Wang, Y. Sun, Y. Jiang, Dalton Trans. 43 (2014) 6631-6642.
[38] G. Li, F. Qin, R. Wang, S. Xiao, H. Sun, R. Chen, J. Colloid Interface Sci. 409 (2013) 43-51.
[39] J. Xiong, G. Cheng, G. Li, F. Qin, R. Chen, RSC Adv. 1 (2011) 1542-1553.
[40] P. Balaz, M. Achimovicova, M. Balaz, P. Billik, Z. Cherkezova-Zheleva, J.M. Criado, F. Delogu, E. Dutkova, E. Gaffet, F.J. Gotor, R. Kumar, I. Mitov, T. Rojac, M. Senna, A. Streletskii, K. Wieczorek-Ciurowa, Chem. Soc. Rev. 42 (2013) 7571-7637.
[41] J. Shang, W. Hao, X. Lv, T. Wang, X. Wang, Y. Du, S. Dou, T. Xie, D. Wang, J. Wang, ACS Catal. 4 (2014) 954-961.
[42] T. Wu, G. Liu, J. Zhao, H. Hidaka, N. Serpone, J. Phys. Chem. B 102 (1998) 5845-5851.
[43] A. Sivakumar, B. Murugesan, A. Loganathan, P. Sivakumar, J. Taiwan Inst. Chem. Eng. 45 (2014) 2300-2306.
[44] A.R. Khataee, M.B. Kasiri, J. Mol. Catal. A: Chem. 328 (2010) 8-26.
[45] J. Liqiang, Q. Yichun, W. Baiqi, L. Shudan, J. Baojiang, Y. Libin, F. Wei, F. Honggang, S. Jiazhong, Sol. Energy Mater. Sol. Cells 90 (2006) 1773-1787.
[46] S.K. Apte, S.N. Garaje, S.D. Naik, R.P. Waichal, B.B. Kale, Green Chem. 15 (2013) 3459-3467.
[47] Z. Shan, X. Lin, M. Liu, H. Ding, F. Huang, Solid State Sci. 11 (2009) 1163-1169.
[48] X. Xiao, C. Liu, R. Hu, X. Zuo, J. Nan, L. Li, L. Wang, J. Mater. Chem. 22 (2012) 22840-22843.
[49] L. Cao, F.-J. Spiess, A. Huang, S.L. Suib, T.N. Obee, S.O. Hay, J.D. Freihaut, J. Phys. Chem. B 103 (1999) 2912-2917.
[50] Q. Xiao, Z. Si, J. Zhang, C. Xiao, X. Tan, J. Hazard. Mater. 150 (2008) 62-67.
[51] L. Chen, S.-F. Yin, R. Huang, Y. Zhou, S.-L. Luo, C.-T. Au, Catal. Comm. 23 (2012) 54-57.
[52] G. Tian, Y. Chen, W. Zhou, K. Pan, C. Tian, X.-r. Huang, H. Fu, Cryst. Eng. Comm. 13 (2011) 2994-3000.
[53] X. Zhang, B. Li, J. Wang, Y. Yuan, Q. Zhang, Z. Gao, L.-M. Liu, L. Chen, Phys. Chem. Chem. Phys. 16 (2014) 25854-25861.